Available online at www.sciencedirect.com

ScienceDirect

Procedia CIRP 94 (2020) 565–570

www.elsevier.com/locate/procedia

11th CIRP Conference on Photonic Technologies [LANE 2020] on September 7-10, 2020

Challenges and opportunities in laser welding of 6xxx high strength aluminium extrusions in automotive battery tray construction

T. Sun*, P. Franciosa, M. Sokolov, D. Ceglarek

WMG, University of Warwick, Coventry CV4 7AL, UK

* Corresponding author. Tel.: +44(0)2476575022; fax: +44(0)2476575022. *E-mail address:* Tianzhu.sun@warwick.ac.uk

Abstract

Laser welding has been increasingly adopted into the automotive sector due to its competitive processing speed, less restrictive single-sided access requirements and improved process flexibility. These benefits notwithstanding, laser welding still remains susceptible to the weld cracking especially for 6xxx high strength aluminium extrusions, which are widely used in the automotive industry for body-in-white and battery tray manufacturing. This paper reviews current challenges and opportunities for construction of battery tray using aluminium alloys with laser welding process. It aims to provide a view on the selection of welding equipment in terms of beam oscillation, power modulation, beam shaping, filler wire and shielding gas, and analyze their impact on joint integrity for 6xxx grades aluminium extrusions. The driving idea is to control the thermal history in and around the molten pool and to modify the chemical composition in the fusion zone to reduce the formation of solidification cracks. Results of the study have shown that the modification of chemical composition by the use of filler wire is currently the most efficient approach to improve joint strength. Further results evidences also showed that beam shaping with adjustable ring mode laser helps to stabilize the keyhole and achieve a wider molten pool and weld interface width. Manufacturing implications are reviewed and discussed throughout the paper.

Keywords: Laser Welding, 6xxx Aluminium Extrusions, Weld Cracks, Beam Oscillation, Power Modulation, Adjustable Ring Mode Laser, Joint Integrity

1. Introduction

Newer regulations and policies which recognize the importance of controlling and reducing carbon emission, air and noise pollution, have accelerated the development of e-mobility technologies in the automotive market with the need for lighter, stronger and cost-effective structures [1]. Li-ion based automotive battery pack is an alternative energy source to internal combustion engines that is increasingly used to power up plug-in hybrid or battery electric vehicles (PHEV/ BEV). The assembly process of a typical automotive battery pack is usually described by: (a) cell fabrication (i.e., electrodes to tab joining); (b) module assembly (i.e., tab to busbar joining); and, (c) pack assembly (i.e., module-to-module connections). A pack is formed by connecting multiple modules with sensors and a controller and then housing it in a case, called tray. Although significant research already exists mapping current joining technologies to manufacturing readiness levels [2], there is a significant gap in understanding needs and requirements for manufacturing of battery trays. Battery tray is the interface between the underbody structure and the road for the housing of battery packs. Its design implies high engineering complexity with multiple requirements such as water/gas tightness, strength, weight distribution and cooling of high-voltage circuits. Fig. 1 shows the typical design of a battery tray, with base plate, cross and side members.

The selection of materials and joining processes for construction of battery tray is a challenging task which must account for both technical performances (i.e., weight, strength and sealing) and manufacturing costs. The current trend in high volume production is to use aluminium battery tray for high range BEVs (more than 250 km before discharge); whereas steel structures are used for low range vehicles. On the other hand, low volume production tends to use composite or multi-material structures.

2212-8271
10.1016/j.procir.2020.09.076

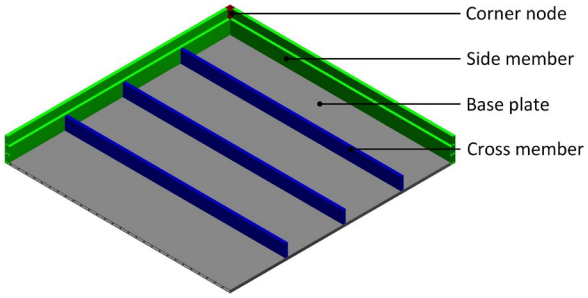

Fig. 1. Typical design of automotive battery tray for electric vehicle.

The results of the survey published at the Automotive Circle EALA2020 conference [3] showed a 30% preference towards the adoption of aluminium alloys for novel solutions to facilitate cheaper and lighter battery tray manufacturing, with laser welding as one preferred joining option, alongside friction stir welding. Tactile Laser Welding (TLW) with the use of filler wire has proven to be a promising joining technology because of benefits such as single side access, reduced heat input and dramatically enhanced processing speed. Furthermore, Remote Laser Welding (RLW) brings additional advantages to TLW such as low operational cost due to the absence of filler wire and shielding gas and increase processing flexibility achieved by the rapid response of laser scanner optics [4,5].

This paper reviews current challenges and opportunity for construction of battery tray using aluminium alloys with both TLW and RLW processes. It aims at providing a critical view on the selection of welding equipment and process parameters (i.e., beam oscillation, power modulation, beam shaping, filler wire and shielding gas) in the context of its impact on optimisation of joint integrity for a set of 6xxx grades Aluminium extrusions.

2. Background

It has been demonstrated that only ~20 kg of aluminium extruded profiles are included in vehicles with internal combustion engines whereas BEVs contain up to 250 kg [6]. The adoption of extruded profiles is one efficient solution to offer excellent strength to weight ratio, design flexibility and modularity and is perceived as a preferred option for manufacturing battery tray. However, the flawless adoption of 6xxx aluminium extrusions is hindered by the following challenges:

(1) *weld porosity* – pores which are trapped in the melting pool reduce weld strength, durability and water/gas tightness;
(2) *part-to-part gaps* – manufacturing tolerances of extruded profiles being welded may lead to unwanted part-to-part gaps. Standard form tolerance of extruded profiles is ±0.8mm across 1m length, which if left uncontrolled can lead to part-to-part gaps of up to 1.6mm [7]; and,
(3) *weld cracks* – these are major weld defects, which occur because of high thermal stresses during solidification and is worsened by high thermal conductivity of aluminium.

Weld porosity is associated with two main phenomena: (a) hydrogen or contaminants that are entrapped in the melting pool and leave voids in the solidified weld; and, (b) collapse of the keyhole during the laser welding process. Compared to steel or ferrous-based alloys, the molten liquid tends to exhibit lower viscosity which turns to unstable equilibrium between capillary pressure inside the keyhole and weight exerted by the molten pool. As a result, keyhole tends to collapse more often which leaves voids in the solidified weld. In recent years, most research has focused on developing effective solutions to improve keyhole stability and maximise the weldability of aluminium alloys. This has been possible with the introduction of laser beam oscillation, power modulation and beam shaping techniques [8]. The combination of beam oscillation and power modulation has also been used to bridge part-to-part gaps with autogenous RLW joining process. Successful reports have developed solutions for sheet metal applications (typical thicknesses are in the range of 1.5 to 2mm), especially for closures and hang-on parts, with fillet lap joint geometry [9,10].

Typically, a total ~30m of weld length is necessary during the construction of a battery tray to join the bottom plate to the side/cross members and corner nodes. This underscores the need for a robust gap bridging control to avoid seam weld discontinuity and meet the target of water/gas tightness. The conceptual approach for gap bridging is based on the observation that as gap increases more material has to drop/melt from the upper part to fill the part-to-part gap. This is obtained by adaptive selection of welding process parameters, such as laser power and beam oscillation amplitude, which facilitate the droplet formation and the bonding with the bottom part. Fig. 2 shows typical weld cross sections obtained with gap bridging during autogenous RLW joining process [10,11].

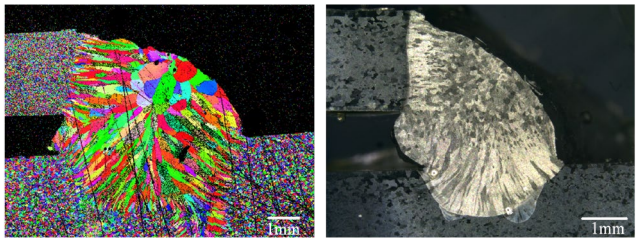

Fig. 2. Typical weld cross-sections obtained with beam oscillation and power modulation during autogenous RLW joining process. Left – 1.5mm upper material thickness, AC170; Right – 2.5mm upper material thickness, AA6060.

Though widely researched, the phenomenon of weld cracking remains a leading challenge during welding of 6xxx aluminium alloys. Modelling and characterization of weld cracking has attracted enormous interest in the laser welding community. Several approaches have been proposed, both theoretical-based and data-driven. The common understanding is that the addition of Si content in Al-Mg-Si alloys extends the critical solidification temperature range where thermal strain excesses material ductility during rapid cooling period after welding [12]. Beside metallurgical aspects, thermal history, mechanical restraints and dynamics of melt pool affect the formation and propagation of weld cracks. For example, Marangoni forces induce flows in the melt pool which help to push the molten liquid between the dendrites and reduce the risk of cracking [13].This paper will focus on solidification cracking phenomenon and discuss the impact of both macro cracks (also called centerline crack) and micro cracks since liquation cracks have rarely been

observed due to the low heat input and narrow HAZ of laser welds [14].

3. Experimental setup & welding configurations

Three high strength Aluminium alloy extrusions, AA6060-T6 (1.5mm) [15], AA6063-T6 (2.5mm) and AA6008-T7 (2.5mm) [16], were studied in this paper and corresponding chemical composition is shown in Table 1.

Table 1. Maximum content (wt. %) of alloying elements of materials.

Material	Si	Fe	Cu	Mn	Mg	Zn	Ti
6008-T7	0.90	0.35	0.30	0.30	0.70	0.20	0.10
6060-T6	0.53	0.30	0.10	0.10	0.60	0.15	0.10
6063-T6	0.60	0.35	0.10	0.10	0.90	0.10	0.10

Beam oscillation is achieved by the motorized mirror and collimator integrated in the WeldMaster Scan&Track remote welding head (YW52 Precitec GmbH, Germany). Temporal beam power modulation is allowed by the analog interface between the laser source and the welding head. Beam shaping is obtained by using the built-in capability of Coherent ARM FL10000 laser system. Adjustable Ring Mode (ARM) laser is a new concept for laser welding due to the independence of controlling the power in the ring laser. The central laser *core* promotes the generation of keyhole, while the *ring* laser ensures a good distribution of temperature thus to control the cooling rate in and around the molten pool [17]. Illustration of key welding parameters is shown in Fig. 3. Table 2 and Table 3 report the details of the laser welding systems and the welding configurations, respectively. AlSi12 filler wire and argon were implemented for those configurations with filler wire and shielding gas. Welded joints were analyzed from the perspectives of weld zone geometry and mechanical property. To evaluate the weld zone geometry, cross-section metallographs were obtained by optical microscope after mechanically grinding and polishing with 9 µm, 3 µm and 1 µm MetaDi supreme solution respectively and then etching in sodium hydroxide (NaOH) solution for 2 minutes. Tensile shear test was performed on specimens 20 mm wide at a constant extension rate of 1mm/min; the maximum linear load (N/mm) was then extracted as indicator of the joint strength. Vickers micro-hardness test was carried out with a load of 0.2 kg and dwell time of 10s to reveal local material strength distribution. Fracture surface of tested specimens was analysed by Hitachi TM3000 tabletop SEM.

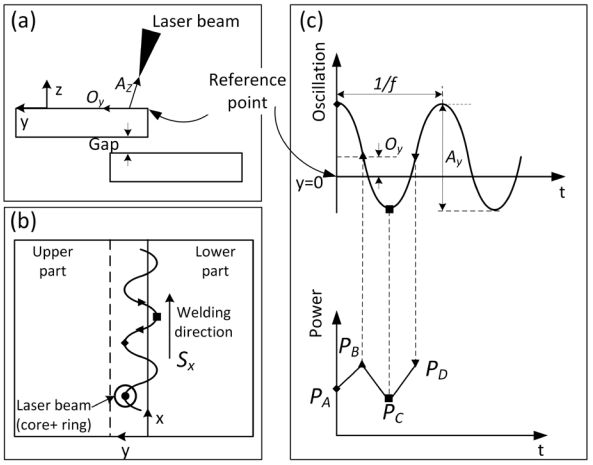

S_x: Robot travel speed [m/min]
f, A_y: Beam oscillation frequency [Hz] and amplitude [mm]
A_Z: Beam focal position offset along beam axis [mm]
O_y: Beam lateral offset [mm]
$P^c_{A,B,C,D}$: Beam power at Core - with modulation [kW]
P^c: Beam power at Core - no modulation [kW]
$P^r_{A,B,C,D}$: Beam power at Ring - with modulation [kW]
P^r: Beam power at Ring - no modulation [kW]

Fig. 3. Illustration of key welding parameters; (a) cross view; (b) top view and; (c) beam oscillation and power modulation [9].

Table 2. Description of laser welding systems.

ID	Laser system	Fiber diameter (µm)	Fiber wavelength (nm)	BPP (mm·mrad)	Max power (kW)	Collimating length (mm)	Focusing length (mm)	Beam diameter at focus (mm)
I	Laserline	150 (core)	1080	6	6.0 (core)	150	300	300
II	Coherent ARM	70 (core) 180 (ring)	1080	16	5.0 (core) 5.0 (ring)	150	300	140 (core) 360 (ring)
III	Coherent ARM	70 (core) 180 (ring)	1080	16	4.0 (core) 4.0 (ring)	100	400	280 (core) 720 (ring)
IV	Coherent Ring only	300 (ring)	1080	8	8.0 (ring)	160	400	750 (ring)

Table 3. Matrix of welding configurations studied in this paper. Note: Laser system ID refers to Table 2.

Set-up	Materials	Beam oscillation	Power Modulation	Beam shaping	Filler wire	Shielding gas	Laser system ID	Motion system	Optics setup
#1	6008-T7	√	√				I	ABB 6700	Precitec WeldMaster
#2	6008-T7	√	√	√			II	ABB 6700	Precitec WeldMaster
#3	6008-T7			√	√	√	III	Kuka KR60 L45	Coherent-Rofin
#4	6008-T7			√	√	√	IV	Kuka KR60 L45	Coherent-Rofin
#5	6060-T6	√	√				I	ABB 6700	Precitec WeldMaster
#6	6060-T6			√	√	√	III	Kuka KR60 L45	Coherent-Rofin
#7	6060-T6			√	√		III	Kuka KR60 L45	Coherent-Rofin
#8	6060-T6			√	√	√	IV	Kuka KR60 L45	Coherent-Rofin
#9	6063-T6	√	√				I	ABB 6700	Precitec WeldMaster
#10	6063-T6	√	√	√			II	ABB 6700	Precitec WeldMaster

4. Results

4.1. Control of centerline cracks

Fig. 4 shows representative weld cross-sections with different edge distances representing the transition from overlap joint (Fig. 4(a)) to fillet lap joint (Fig. 4(a)).

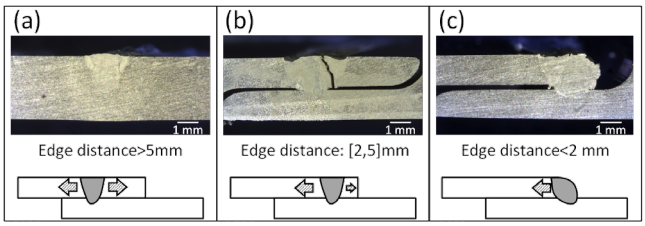

Fig. 4. Representative cross-sections of 6063-T6 aluminium alloy welds with different edge distances - (a) more than 5mm (overlap joint configuration); (b) within the range of 2-5mm; and, (c) less than 2 mm (fillet lap joint configuration). Heat dissipation in each case is illustrated by the arrow and the size of arrow represents the level of heat dissipation.

Results show that centerline cracks can be effectively controlled by adequate design of edge distance. Edge distances less than 2mm or more than 5mm were found less sensitive to centerline crack. For edge distance > 5mm, there is enough material on both sides of fusion zone to accommodate the heat dissipation. It eventually leads to a symmetrical thermal field and low level of thermal strain in the fusion zone. When the fusion zone is closer to the edge with edge distance within [2, 5]mm, thermal field tends to be asymmetrical and skewed toward left, and generates residual thermal strains which may exceed the critical strength in the mushy zone. For edge distance < 2mm, there will be a transition from multi-directional solidification to uni-directional solidification, which is less prone to centerline crack susceptibility [18]. Therefore, from the perspective of reducing crack susceptibility and also benefits such as seam tracking and part-to-part gap monitoring for adaptive control, fillet lap joint configuration was chosen as preferred option.

Though fillet lap weld helps to reduce centerline cracks, optimization of welding parameters is essential. Fig. 5 shows two AA6060-T6 fillet lap cross-sections with different welding parameters referring to the case of un-optimized (a) and optimized (b) welds. With A_y=1.6mm and O_y = -0.1mm (laser beam shifted towards to the lower part) the weld seam shows a concave shape with a centerline crack which extends throughout the fusion zone. This is imputed to the higher thermal strain resulted from the narrow fusion zone and resultant high cooling rate. Conversely, with A_y=2.6mm and O_y = 0.3mm (laser beam shifted towards to the upper part) the weld seam significantly improves and appears wider and convex, and no evidence of centerline crack. The reduced weld penetration in Fig. 5(b) is associated to the reduction of laser power on the point C (P_C^c=2.9kW). Yet, internal micro cracks need to be investigated further.

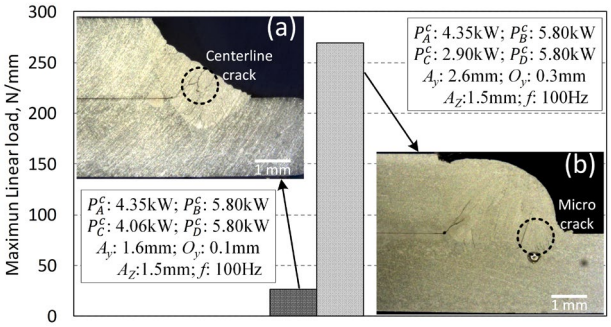

Fig. 5. Improvement of joint strength and suppression of centerline cracks by optimisation of welding parameters with welding set-up #5 at S_x=4m/min.

4.2. Control of micro cracks

Fig. 6 shows representative cross-sections in all welding configurations shown in Table 3, with the detailed welding process parameters in Table 4. After selecting the of optimized welding parameters, all cross-sections show no centerline cracks. However, internal micro cracks are visible in set-up #1, #5 and #9 (with the use of beam oscillation and power modulation), and also in set-up #2 and #10 (with the use of beam shaping). They are located in the region adjacent to the boundary between the fusion zone and heat affected zone, and also towards the tip of the fusion zone. It is therefore reasonable to conclude that pure modification of thermal history (either by temporal power modulation or spatial laser power distribution) is not sufficient to reach crack-free welds. Only the welds in set-up #3, #4, #6 to #8 (with the use of AlSi12 filler wire) show no micro cracks. This supports the fact that the modification of chemical

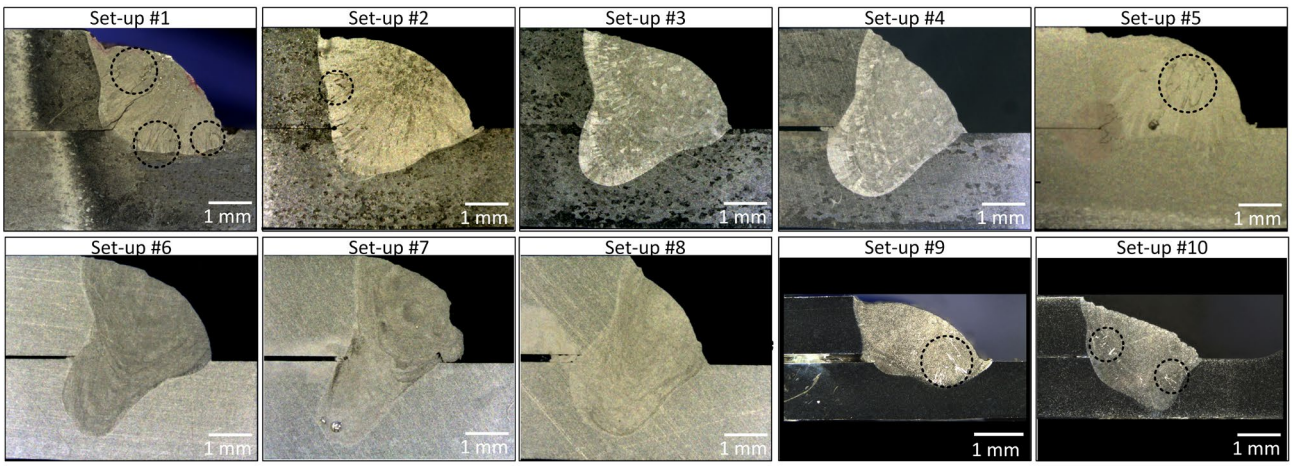

Fig. 6. Representative cross-sections in all welding configurations in Table 3 with micro cracks addressed by dashed circle.

Table 4. Detailed welding process parameters of the set-ups shown in Table 3.

Set-up	Power at @Core (kW)	Power at @Ring (kW)	S_x (m/min)	Filler wire feed rate (m/min)	Gas feed rate (L/min)	O_y (mm)	A_Z (mm)	A_y (mm)	f (Hz)
#1	$P^c_{A,B,C,D}$:4.8, 6.0, 2.7, 6.0	N/A	4.0	N/A	N/A	0.7	2.5	1.7	100
#2	$P^c_{A,B,C,D}$:1.5, 1.5, 1.5, 1.5	$P^r_{A,B,C,D}$:5.0, 5.0, 1.5, 5.0	4.0	N/A	N/A	0.6	2.0	1.5	100
#3	P^c:1.4	P^r:4.0	4.0	6.0	15	0.0	N/A	N/A	N/A
#4	N/A	P^r:6.5	6.0	6.5	15	0.0	N/A	N/A	N/A
#5	$P^c_{A,B,C,D}$:4.9, 5.8, 3.8, 5.8	N/A	4.0	N/A	N/A	0.7	1.5	2.6	100
#6	P^c:1.2	P^r:4.0	3.5	6.0	15	0.0	N/A	N/A	N/A
#7	P^c:1.4	P^r:4.0	4.0	6.0	N/A	0.0	N/A	N/A	N/A
#8	N/A	P^r:7.0	6.5	7.0	15	0.0	N/A	N/A	N/A
#9	$P^c_{A,B,C,D}$:2.6, 5.1, 2.3, 5.1	N/A	4.0	N/A	N/A	0.4	2.0	1.8	100
#10	$P^c_{A,B,C,D}$:1.4, 3.0, 1.1, 3.0	$P^r_{A,B,C,D}$:0.3, 0.3, 0.3, 0.3	4.0	N/A	N/A	0.2	2.0	1.8	100

composition of the fusion zone with the addition of Si enhances the weldability of the alloy. It should be also noted that no significant difference was found between ring-only mode (set-up #4 and #8) and core & ring mode (set-up #3 and #6) in terms of presence of micro cracks when filler wire is used. Fig. 7 compares the hardness distribution of the two weld configurations obtained with and without filler wire for AA6008-T7. Results show a significant increase of the hardness in the fusion zone when filler wire is adopted. This is mainly due to the change of chemical composition in the fusion zone that facilitates the formation of strengthening precipitates.

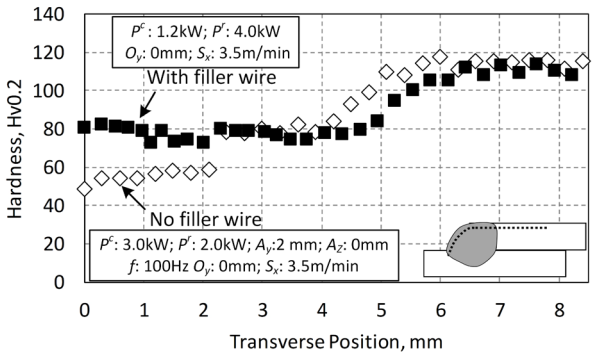

Fig. 7. Transverse hardness distributions of 6008-T7 welds after one-week natural ageing. (Note that measurement indent has an offset of 0.5mm from the outline of cross-section)

Fig. 8 summarizes the weld joint strength in all welding configurations shown in Table 3, with detailed welding process parameters presented in Table 4. Taking 6008-T7 welds as example, it is noted that beam oscillation + power modulation (#1) and beam shaping (#2) have limited effect on the joint strength. In comparison, the improvement is more pronounced by the use of filler wire (#3, #4). More surprisingly, same level of joint strength was achieved by the use of ring-only mode even at a higher welding speed of 6 and 6.5 m/min, compared to results at 4m/min.

To better understand the effect of filler wire on joint strength, fracture surface after tensile test was determined and shown in Fig. 9. Dimples shown in each fracture surface indicates the ductile fracture failure. However, cavities in Fig. 9 (a) and (b) reveal the presence of micro cracks and pores, which can provide a local strain concentration and lead to the rapid propagation of failure. When adding filler wire, distribution of dimples on fracture surface is more uniform (Fig. 9(c)) which is indicator of significant reduction of number of micro cracks. Therefore, it is reasonable that distinctive increase in joint strength by the use of filler wire is attributed to two phenomena: the increase of hardness in the fusion zone; and, the reduction of welding defects such as micro cracks and pores. Furthermore, experimental results support conclusion that shielding gas can be used to improve joint strength by improving seam surface finish and strengthening the bonding. More research will be carried out in the future to better understand the impact of shielding gas.

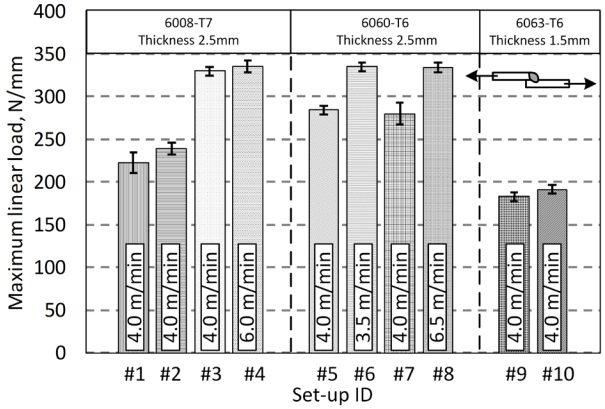

Fig. 8. Summary of weld joint strength (lap shear test) produced in different welding configuration after one-week natural ageing.

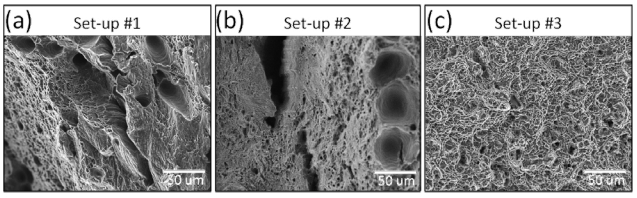

Fig. 9. Representative fracture surface after tensile test in 6008-T7 welds produced in the welding configuration (a) set-up #1, (b) set-up #2 and (c) set-up #3.

5. Conclusions and final remarks

The paper discussed challenges and technological solutions to laser welding of 6xxx aluminium extrusions. Numbers of welding equipment have been tested, with capability for beam oscillation, power modulation, beam shaping, filler wire and shielding gas. Key findings are listed below:

- Centerline cracks can be effectively avoided by the use of fillet lap joint configuration integrated with beam oscillation and power modulation;
- Modification of thermal history by beam oscillation, power modulation and beam shaping tend to reduce

Table 5. Manufacturing implications and competitive benefits of welding configurations and technological capabilities (case of fillet lap joint).

Technological capability	Advantages	Disadvantages
Beam Oscillation Power Modulation	• Gap bridging up to 50% of upper material thickness • Avoidance of centerline cracks • Compatible with optical seam tracking	• No control of micro-cracking
Beam Shaping	• Reduction of weld pores • Localised in-process thermal treatment • Improved weld width and seam smoothness • Improved joint strength by ring-only laser beam	• Limited control of micro-cracking (further work required to understand the full capability)
Filler wire	• Able to deliver crack-free weld • Reduction of weld pores • Improved joint strength	• Increased system complexity • Need for consumables • Synchronisation of robot, wire feeder, laser controller and optical setup may be cumbersome • Insufficient control of laser beam alignment • Reduced welding speed
Shielding gas	• Reduction of weld pores • Improved seam smoothness	• Increased system complexity • Need for consumables

number and distribution of micro cracks; however, they are not sufficient to reach a crack-free weld;

- Addition of filler wire is so far the most efficient solution to control micro cracks and improve joint strength. An improvement of up to 40% in joint strength has been observed compared to the case without filler with the use of beam oscillation and power modulation;
- Same level of joint strength was achieved by the use of ring-only mode even at higher welding speed of 6 and 6.5m/min, compared to results at 4m/min obtained with filler wire.

Table 5 summarizes the competitive benefits of each technological capability. Future work will be devoted to study:

- feasibility of welding at higher welding speed – currently, the maximum tested speed is 6.5m/min – with the aim to increase production efficiency;
- impact of ring-only mode (with and without filler wire) on weld quality and control of micro-cracking; and,
- technological feasibility to integrate in-process monitoring system with the ultimate goal of achieving in-process closed-loop quality control system.

Acknowledgements

This study was partially supported by the WMG HVM Catapult, APC UK project: Chamaeleon - New lightweight Materials and Processing Technologies for Common Lightweight Architecture of Electric and Hybrid Powertrain Systems, and the Innovate UK IDP15 project LIBERATE: Lightweight Innovative Battery Enclosures using Recycled Aluminium Technologies. We greatly acknowledge the technical support of Coherent during the welding trials.

References

[1] González Palencia JC, Furubayashi T, Nakata T. Energy use and CO2 emissions reduction potential in passenger car fleet using zero emission vehicles and lightweight materials. Energy 2012, 48, 548–565.

[2] Kölmel A, Sauer A, Lanza G. Quality-oriented production planning of battery assembly systems for electric mobility. Procedia CIRP 2014, 23, 149–154.

[3] Lasers go E-mobile – industry survey. In Proceedings of the EALA 2020 - Automotive Circle; Bad Nauheim.

[4] Ceglarek D, Colledani M, Váncza J, Kim DY, Marine C, Kogel-Hollacher M, Mistry A, Bolognese L. Rapid deployment of remote laser welding processes in automotive assembly systems. CIRP Ann. - Manuf. Technol. 2015, 64, 389–394.

[5] Franciosa P, Sun T, Ceglarek D, Gerbino S, Lanzotti A. Multi-wave light technology enabling closed-loop in-process quality control for automotive battery assembly with remote laser welding. In Multimodal Sensing: Technologies and Applications, vol. 11059, p. 110590A. International Society for Optics and Photonics, 2019.

[6] Blendl W, Cuppoletta N. Trend towards e-Mobility accelerates Aluminium Use Available online: https://www.aluminium-messe.com/en/ALUMINIUM-2020/Trend-towards-e-Mobility-accelerates-Aluminium-Use/879/.

[7] BS EN 12020-2:2016 Aluminium and aluminium alloys. Extruded precision profiles in alloys EN AW-6060 and EN AW-6063. Tolerances on dimensions and form. Bsi 2016.

[8] Sokolov M, Franciosa P, Botros Al, Ceglarek D, Road GH. Keyhole Mapping to Enable Closed-Loop Weld Penetration Depth Control for Remote Laser Welding of Aluminium Components Using Optical Coherence Tomography. Int. Congr. Appl. Lasers Electro–Optics Conf. 2019.

[9] Müller A, Goecke SF, Sievi P, Albert F, Rethmeier M. Laser beam oscillation strategies for fillet welds in lap joints. Phys. Procedia 2014, 56, 458–466.

[10] Franciosa P, Serino A, BotrosAl, Ceglarek D. Closed-loop gap bridging control for remote laser welding of aluminum components based on first principle energy and mass balance. J. Laser Appl. 2019, 31, 022416.

[11] Franciosa P, Sokolov M, Sinha S, Sun T, Ceglarek, D. Deep Learning Enhanced Digital Twin for Remote laser Welding of Aluminium Structures. CIRP Ann. Manuf. Technol. 69/1.

[12] Dudas HJ. Preventing weld cracks in high strength aluminum alloys. Weld. J. 1966, 45, 3.

[13] Langrieger H, Krafft F, Mensinger M, Oefele F. Thermomechanical analysis of the formation of hot cracks in remote laser welded aluminium fillet welds. J. Laser Appl. 2016, 28, 022414.

[14] Zhao H, White DR, DebRoy T. Current issues and problems in laser welding of automotive aluminium alloys. Int. Mater. Rev. 2003

[15] Aalco Aluminium Alloy - Commercial Alloy - 6060 - T5 Extrusions Available online: http://www.aalco.co.uk/datasheets/Aluminium-Alloy-6060-T5--Extrusions_144.ashx.

[16] MakeeltFrom 6008 (AlSiMgV, A96008) Aluminum Available online: https://www.makeitfrom.com/material-properties/6008-AlSiMgV-A96008-Aluminum.

[17] Wang L, Mohammadpour M, Yang B, Gao X, Lavoie JP, Kleine K, Kong F, Kovacevic R. Monitoring of keyhole entrance and molten pool with quality analysis during adjustable ring mode laser welding. Appl. Opt. 2020, 59, 1576–1584.

[18] Stritt P, Weber R, Graf T, Mueller S, Weberpals JP. New hot cracking criterion for laser welding in close-edge position. ICALEO 2012 - 31st Int. Congr. Appl. Lasers Electro-Optics 2012, 357, 357–366.